LETTER

doi:10.1038/nature11341

# Electronic read-out of a single nuclear spin using a molecular spin transistor

Romain Vincent[1], Svetlana Klyatskaya[2], Mario Ruben[2,3], Wolfgang Wernsdorfer[1] & Franck Balestro[1]

**Quantum control of individual spins in condensed-matter devices is an emerging field with a wide range of applications, from nanospintronics[1,2] to quantum computing[3]. The electron, possessing spin and orbital degrees of freedom, is conventionally used as the carrier of quantum information in proposed devices[4,5,6,7,8,9]. However, electrons couple strongly to the environment, and so have very short relaxation and coherence times. It is therefore extremely difficult to achieve quantum coherence and stable entanglement of electron spins. Alternative concepts propose nuclear spins as the building blocks for quantum computing[10], because such spins are extremely well isolated from the environment and less prone to decoherence. However, weak coupling comes at a price: it remains challenging to address and manipulate individual nuclear spins[11,12,13,14]. Here we show that the nuclear spin of an individual metal atom embedded in a single-molecule magnet can be read out electronically. The observed long lifetimes (tens of seconds) and relaxation characteristics of nuclear spin at the single-atom scale open the way to a completely new world of devices in which quantum logic may be implemented.**

Single-shot read-out of a single nuclear spin has remained elusive until the past few years, when it was achieved on a single nitrogen-vacancy defect centre in diamond[15]. The use of single-molecule magnets (SMMs) has also been proposed as a structural basis for nanospintronics[16] and quantum information[9]. The argument in favour of molecular building blocks for quantum computing is based on the possibility of synthesizing billions of perfectly identical SMMs, which can be integrated in devices by bottom-up approaches and for which the intrinsic magnetic properties and the environment can be chemically engineered. Moreover, experiments on an assembly of SMMs have already shown that: SMMs are characterized by a large spin ground state combined with uniaxial magnetic anisotropy leading to two stable spin orientations; quantum phenomena such as quantum tunnelling of the magnetization (QTM)[17,18] and quantum phase interference[19] can be observed; and spin-state oscillations can be made coherent[20,21] for a time on the order of 1 μs. To achieve a longer coherence time, experiments must be done on the single-molecule level, avoiding interactions between SMMs. However, it is still difficult to detect single spin states in an SMM. Towards this goal, transport measurements have been made using scanning tunnelling microscopy (STM)[22,23], and SMMs have been studied in a transistor-like configuration using electromigrated junctions[24,25] or carbon-nanotube transistors[26]. So far, only signatures accounting for the electronic magnetic moment have been addressed, and there has been no quantitative comparison with the expected theoretical magnetic behaviour of an individual SMM.

Here, transport measurements taken through a single bis(phthalocyaninato)terbium(III) SMM ($TbPc_2$, Fig. 1) are studied in a three-terminal geometry obtained by electromigration[27]. $TbPc_2$ is a lanthanide SMM, in which the magnetic moment is carried by a single $Tb^{3+}$ metal ion sandwiched between two organic phthalocyanine (Pc) ligands. We used this particular SMM for the several reasons. It has been reported that $TbPc_2$ SMMs conserve both their structural integrity and their magnetic properties even when sublimated at 820 K on a copper surface[28]. The redox state of the $Tb^{3+}$ ion is very stable; that is, it is very unlikely that a current can flow through the $Tb^{3+}$ ion (see Supplementary Information). The two Pc ligands have a conjugated π system, which can easily conduct electrons. Owing to strong spin–orbit coupling and the Pc ligand fields, $TbPc_2$ has a magnetic ground state of $J = 6$ and a strong uniaxial magnetic anisotropy (Ising-like, Fig. 1a). The ground-state doublet $J_z = \pm 6$ is well isolated

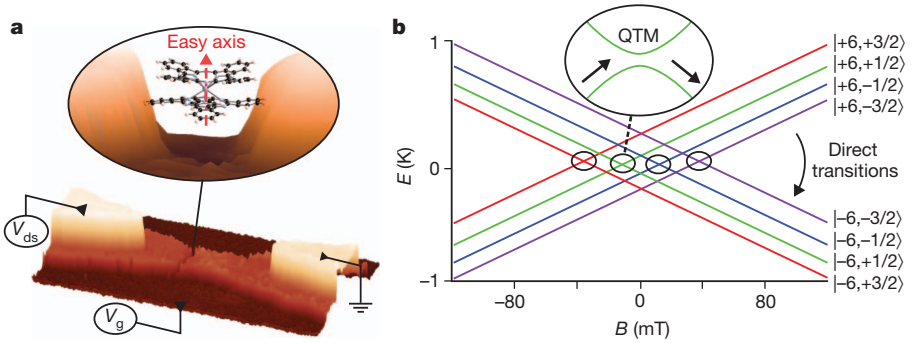


**Figure 1 | Geometry of the molecular spin transistor and magnetization reversal processes. a**, Three-dimensional extrapolation of a scanning-electron-microscope image showing the most favourable structure of the single-molecule-based transistor. A schematic zoom into the nano gap shows the molecular structure of the $TbPc_2$ SMM and its easy axis. The charge state of the ligand read-out dot can be controlled by the gate voltage, $V_g$, and the voltage difference between the electrodes is controlled through the drain-source voltage, $V_{ds}$. **b**, Zeeman diagram presenting the energy, $E$, of the two ground states, $J_z = \pm 6$, as a function of the magnetic field ($B$). The two ground states are each split into four different sub-states owing to the hyperfine coupling with the nuclear spin of $I = 3/2$. Coloured lines denote the $I_z$ components of the nuclear spin states: purple, −3/2; blue, −1/2; green, 1/2; and red, 3/2. Two processes are responsible for the magnetization reversal. In small magnetic fields, QTM can occur at the avoided energy-level crossings with the same $I_z$ but opposite $J_z$, indicated by the black circles. In higher fields, a direct relaxation process can lead to the reversal of $J$.

[1]Institut Néel, CNRS et Université Joseph Fourier, BP 166, F-38042 Grenoble Cedex 9, France. [2]Institute of Nanotechnology, Karlsruhe Institute of Technology, 76344 Eggenstein-Leopoldshafen, Germany. [3]Institut de Physique et Chimie des Matériaux de Strasbourg, CNRS-Université de Strasbourg, 67034 Strasbourg, France.

from the excited states by an energy gap of a few hundred kelvin[29]. The excited states can thus be neglected for experiments carried out at low temperatures (less than 5 K) and small magnetic fields (less than 10 T). The ligand fields also induce transverse magnetic anisotropy, which is responsible for the coupling of the two states of the doublet $J_z = \pm 6$, so that energy-level crossings are avoided[29] (see the black circles in the Zeeman diagram of Fig. 1b). Finally, because of strong hyperfine coupling with the nuclear spin $I = 3/2$ of the $Tb^{3+}$ ion, each ground state $J_z = \pm 6$ is split into four states (Fig. 1b).

Within the low-temperature regime, the magnetization reversal of a $TbPc_2$ SMM takes place through two different processes. In small magnetic fields, QTM at the four avoided level crossings (see above) is the main mechanism[29], whereas in higher magnetic fields, relaxation processes can be direct, involving non-coherent tunnelling events combined with phonon emission. QTM of a $TbPc_2$ SMM has been observed in a supramolecular carbon-nanotube SMM spin-valve geometry[26], but the signature of the hyperfine coupling could not be accessed, owing to the background noise induced by the surrounding $TbPc_2$ SMMs. Here, we show that by detecting the reversal of the electronic magnetic moment of the $TbPc_2$ SMM, we can produce an electronic read-out of the four nuclear spin states of a single $Tb^{3+}$ ion with high efficiency and in perfect quantitative agreement with the theoretical predictions[29]. Furthermore, we estimate the lifetimes and the temperature of a single nuclear spin.

Transport measurements through a single $TbPc_2$ SMM have been taken previously by scanning tunnelling spectroscopy (STS) experiments[22], for which electronic transport occurred through the Pc ligands and exhibited Coulomb blockade and Kondo effects depending on its charge state (spin states $S = 0$ or 1/2). However, no signature of the magnetic moment carried by the $Tb^{3+}$ ion was observed in this experiment. To detect the reversal of the magnetic moment, and to produce the electronic read-out of the $Tb^{3+}$ nuclear spin states, we inserted the $TbPc_2$ SMM directly into a gold junction obtained by the electromigration technique (see Fig. 1a and Methods). The differential conductance, $dI/dV$, as the function of the drain-source voltage, $V_{ds}$, and the gate voltage, $V_g$, is presented in Fig. 2a. It exhibits a single charge-degeneracy point with a weak spin $S = 1/2$ Kondo effect. A detailed study of the Kondo peak as a function of the applied magnetic field is presented in the Supplementary Information. A ferromagnetic exchange interaction of about 0.35 T was measured between the spin 1/2 of the quantum dot and the magnetic moment carried by the $Tb^{3+}$ ion. Alternative coupling mechanisms (dipolar, magneto-Coulomb, mechanical, flux) are discussed in the Supplementary Information, but the relatively high value of the exchange interaction means that it should be the major contribution to the coupling mechanism, and that the quantum dot is spatially located close to the $Tb^{3+}$ ion. This is indirect proof that the electronic transport occurs through the aromatic Pc ligands, and that the most favourable geometric configuration is the one depicted in Fig. 1a. To summarize: the Pc ligands form a molecular quantum dot and the anisotropic magnetic moment of the $Tb^{3+}$ ion is coupled to the electron path only indirectly, mainly through a ferromagnetic exchange interaction; the presence of a gate allows fine-tuning from the Coulomb blockade to the Kondo regime of the molecular quantum dot; the magnetic properties of the $Tb^{3+}$ ion are then independent of the charge state of the Pc quantum dot (see Supplementary Information); and owing to the exchange coupling, we can use the Pc ligands as a read-out quantum dot to detect the reversal of the electronic magnetic moment carried by the $Tb^{3+}$ ion spin dot.

To produce the electronic read-out of the single nuclear spin carried by the spin dot, we chose experimental conditions close to the charge-degeneracy point ($V_g = -0.9$ V and $V_{ds} = 0$ V in Fig. 2a, see Supplementary Information). When sweeping the magnetic field from negative to positive values, we observed a single abrupt jump of the differential conductance, which reversed when we swept the field in the opposite direction (Fig. 2b). Our detailed studies (see below) showed that these jumps can be accounted for by the reversals of the $Tb^{3+}$ magnetic moment, which slightly influence the chemical potential of the read-out quantum dot through the magnetic interactions

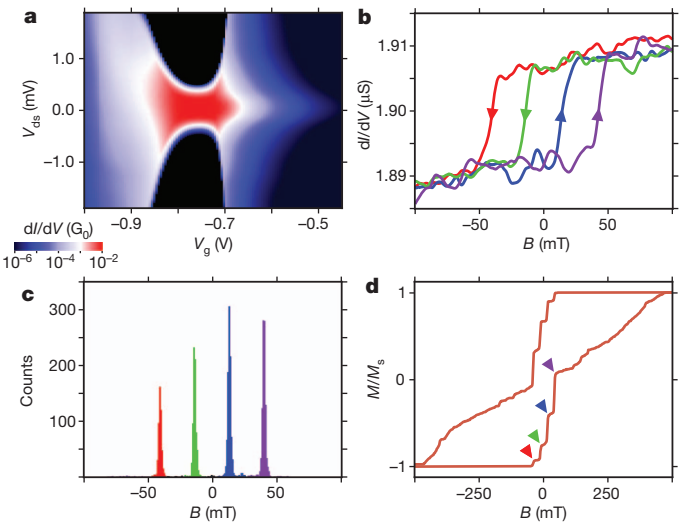


**Figure 2 | Conductance characteristics and electronic read-out procedure.** **a**, Stability diagram of the Pc read-out quantum dot exhibiting the differential conductance, $dI/dV$, in units of the quantum of conductance, $G_0$, as a function of gate voltage, $V_g$, and bias voltage, $V_{ds}$, at 0.1 K. **b**, d$I$/d$V$ measurements for a given working point ($V_g = -0.9$ V; $V_{ds} = 0$ V) as function of the magnetic field, $B$. The arrows indicate the field-sweep direction. Abrupt jumps in the differential conductance, attributed to the switching of the $Tb^{3+}$ magnetic moment, are visible for all traces of $B$, showing a clear hysteresis in the d$I$/d$V$ characteristics. **c**, Histogram of switching field obtained for 11,000 field sweeps showing four preferential field values that are assigned to QTM events. **d**, Normalized hysteresis loop of a single $TbPc_2$ SMM obtained by integration of 1,000 field sweeps and performed for trace and retrace on a larger magnetic-field range than in **c**. The four arrows on the trace curve show the four preferential field values associated to QTM (red, −40 mT; green, −14 mT; blue, 14 mT; purple, 40 mT).

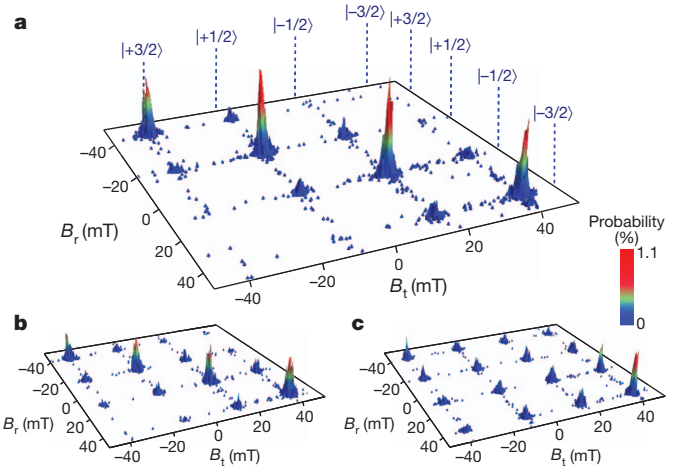


**Figure 3 | Transition matrix of the QTM events as a function of the waiting time.** The switching fields of the $Tb^{3+}$ magnetic moment of subsequent field sweeps are plotted in two-dimensional histograms for three waiting times, $t_w$: **a**, $t_w = 0$ s; **b**, $t_w = 20$ s; and **c**, $t_w = 50$ s. The two axes correspond to the trace and retrace field sweeps, $B_t$ and $B_r$, respectively. Two successive measurements with the same nuclear spin states are situated on the diagonal of the matrix, whereas the off-diagonal positions correspond to nuclear spin-state changes of $\Delta m_I = \pm 1, \pm 2$ and $\pm 3$. The predominance of diagonal terms up to $t_w = 20$ s indicates the long level lifetime of the nuclear spin states. For $t_w = 50$ s, the diagonal terms vanish owing to nuclear spin-flip processes. Furthermore, the high amplitude of the bottom-right ($B_t = B_r = 40$ mT) matrix element accounts for the relaxation of the nuclear spin towards a thermal equilibrium.

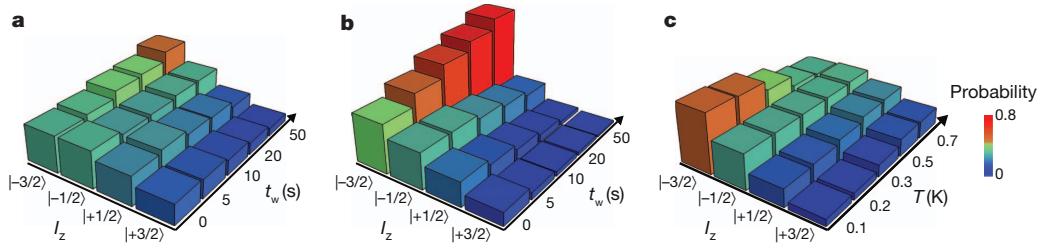


**Figure 4 | Spin-flip dynamics and nuclear spin-state occupancy of the $Tb^{3+}$ nuclear spin states.** Evolution of the nuclear spin-state occupancy as a function of the waiting time, $t_w$, for two different working points: **a**, gate voltage $V_g = -0.9$ V; and **b**, $V_g = -0.1$ V (both at bias voltage $V_{ds} = 0$ V). The measurements clearly show that the populations evolve towards different thermal equilibriums. **c**, Spin dynamics for a fixed waiting time of 10 s, as a function of temperature, $T$. With increasing temperature, the population of the different spin states evolves towards equal occupancy.

(see Supplementary Information). We took subsequent measurements of the reversal as a function of the magnetic-field angle in a dilution refrigerator equipped with a home-made three-dimensional vector magnet. We were thus able to align the field-sweep direction accurately along the easy axis of the $TbPc_2$ SMM (see Supplementary Information).

We obtained the reversal statistics of the magnetization by sweeping the magnetic field back and forth at $0.05\,T\,s^{-1}$ and measuring histograms of the switching fields. We present a typical example in Fig. 2c, showing four preferential magnetic-field values. These are in perfect quantitative agreement with theoretical predictions[29] of QTM of a $Tb^{3+}$ magnetic moment at the four avoided energy-level crossings with the nuclear spin states $|3/2\rangle$, $|1/2\rangle$, $|-1/2\rangle$ and $|-3/2\rangle$ (Fig. 1b). Moreover, the histograms of the four switching fields do not overlap; this shows the high efficiency of this electronic read-out procedure. The field integration of the normalized switching histograms yields the magnetic hysteresis loop (Fig. 2d), which is in excellent accordance with micro-SQUID measurements of assemblies of $TbPc_2$ SMMs (see Supplementary Information and ref. 29). In higher magnetic fields, the reversal of the magnetization occurs stochastically, as predicted for a direct relaxation process involving a non-coherent tunnelling event combined with a phonon emission.

The lifetimes of the four nuclear spin states could be measured by studying the correlations between subsequent measurements as a function of the waiting time, $t_w$, between field sweeps. Figure 3 presents two-dimensional histograms (transition matrices) obtained from 22,000 field sweeps. The two axes correspond to the trace and retrace field sweeps, $B_t$ and $B_r$. Two subsequent measurements with the same nuclear spin states are situated on the diagonal of the matrix; the off-diagonal positions correspond to nuclear spin state changes of $\Delta m_I = \pm 1$, $\pm 2$, and $\pm 3$. For zero waiting time ($t_w = 0$ s, Fig. 3a), the diagonal positions are predominant, highlighting the robustness of the nuclear spin states; that is, indicating long level lifetimes for the individual $Tb^{3+}$ nuclear spin states. The diagonal positions persist even for a waiting time of $t_w = 20$ s (Fig. 3b). However, for $t_w = 50$ s, the off-diagonal positions start to be populated, which suggests the occurrence of nuclear spin–flip processes during the waiting time (Fig. 3c). From this series of measurements, we conclude that the level lifetime of the nuclear spin states is on the order of tens of seconds, confirming that the invasiveness of the measurement procedure is low (see Supplementary Information).

More detailed insight into the spin–flip dynamics of an individual nuclear spin can be gained by measuring the population of nuclear spin states as a function of waiting time and temperature (Fig. 4). To this end, we determined the nuclear spin-state occupancy for two different working points corresponding to two different charge states of the read-out quantum dot ($V_g = -0.9$ V in Fig. 4a and $V_g = -0.1$ V in Fig. 4b, both at $V_{ds} = 0$ V). It is clear that the state occupancy, relaxing towards a thermal equilibrium, depends heavily on the transport characteristics (the current flowing through the Pc quantum dot and/or the electrostatic environment modulated by the gate voltage). Indeed, the electron tunnelling through the Pc-ligands read-out dot gives rise to small fluctuations of the local electric field, which could modify nuclear spin–flip processes through the quadrupole interaction[30]. A detailed study addressing this problem is in progress, and beyond the scope of the work presented here. We also determined the population of nuclear spin states as a function of the temperature (Fig. 4c). The strong temperature dependence of this occupancy demonstrates that a single nuclear spin can be thermalized down to at least 0.2 K, which is close to the electronic temperature of our dilution refrigerator (0.08 K).

In conclusion, we have performed electronic transport studies on a $TbPc_2$ SMM in a transistor-like set-up, taking measurements of a single nuclear spin. Our experimental read-out procedure relies on the highly efficient detection of the QTM of the electronic magnetic moment at particular values of the magnetic field corresponding to the four avoided energy-level crossings; this is in perfect quantitative agreement with theoretical predictions. Using this procedure, the dynamics of the four different nuclear spin states of a single $Tb^{3+}$ ion could be electronically determined. The observation of energy-level lifetimes on the order of tens of seconds opens the way to coherent manipulations of a single nuclear spin. Moreover, because of the different energy-level spacing that originates from the nuclear quadrupole interaction term (see Supplementary Information), this particular device is presumed to be an excellent candidate to perform the Grover algorithm. Indeed it has been proposed that the coherent manipulation of a nuclear spin $I = 3/2$ can be performed through a multiphoton process using this algorithm[31]. It was predicted that the greater the quadrupolar constant, the better the implementation of the algorithm would be. Note that the value presented in ref. 31 was three orders of magnitude smaller than the value presented here ($P = 0.013\,cm^{-1}$). Thus, the demonstrated possibility of addressing and detecting single nuclear spin states using the QTM of SMMs, in combination with the observation of long energy-level lifetimes, opens up a bright new world of nanospintronics with integrated memory, logics and possibly quantum logics.

## METHODS SUMMARY

The single-molecule transistor was prepared by blow-drying a dilute toluene solution of the $TbPc_2$ molecule onto a gold nanowire on an $Au/HfO_2$ gate fabricated through atomic-layer deposition. Before the solution was blow-dried, the electrodes were cleaned with acetone, ethanol, isopropanol solution and oxygen plasma. The connected sample was enclosed in a high-frequency, low-temperature filter, consisting of a thermocoax microwave filter and $\pi$ filters, anchored to the mixing chamber of a dilution refrigerator with a base temperature of about 0.05 K. The molecule-coated nanowire was then broken by electromigration, using a voltage ramp at 4 K. The electromigration technique used real-time electronics to increase the yield of coupling a single molecule to the electrodes.

Transport measurements were taken using a lock-in amplifier in a dilution refrigerator with an electronic temperature of about 0.08 K. It was equipped with a home-made three-dimensional vector magnet, allowing us to sweep the magnetic field in three dimensions at rates up to $0.2\,T\,s^{-1}$.

**Received 9 April; accepted 19 June 2012.**

1. Awschalom, D. D., Loss, D. & Samarth, N. *Semiconductor Spintronics and Quantum Computation* (Springer, 2002).

2. Zutic, I., Fabian, J. & Das Sarma, S. Spintronics: fundamentals and applications. *Rev. Mod. Phys.* **76,** 323–410 (2004).
3. Nielsen, M. A. & Chuang, I. L. *Quantum Computation and Quantum Information* (Cambridge Univ. Press, 2000).
4. Loss, D. & DiVincenzo, D. P. Quantum computation with quantum dots. *Phys. Rev. A* **57,** 120–126 (1998).
5. Imamoglu, A. *et al.* Quantum information processing using quantum dot spins and cavity QED. *Phys. Rev. Lett.* **83,** 4204–4207 (1999).
6. Eble, B. *et al.* Hole–nuclear spin interaction in quantum dots. *Phys. Rev. Lett.* **102,** 1–4 (2009).
7. Jelezko, F., Gaebel, T., Popa, I., Gruber, A. & Wrachtrup, J. Observation of coherent oscillations in a single electron spin. *Phys. Rev. Lett.* **92,** 1–4 (2004).
8. Vrijen, R. *et al.* Electron-spin-resonance transistors for quantum computing in silicon-germanium heterostructures. *Phys. Rev. A.* **62,** 1–10 (2000).
9. Leuenberger, M. N. & Loss, D. Quantum computing in molecular magnets. *Nature* **410,** 789–793 (2001).
10. Kane, B. E. A silicon-based nuclear spin quantum computer. *Nature* **393,** 133–137 (1998).
11. Chuang, I. L., Gershenfeld, N. & Kubinec, M. Experimental implementation of fast quantum searching. *Nature* **393,** 143–146 (1998).
12. Chuang, I. L., Vandersypen, L. M. K., Zhou, X., Leung, D. W. & Lloyd, S. Experimental realization of a quantum algorithm. *Phys. Rev. Lett.* **80,** 3408–3411 (1998).
13. DiVincenzo, D. P. Two-bit gates are universal for quantum computation. *Phys. Rev. A.* **51,** 1015–1022 (1995).
14. Berman, G. P., Doolen, G. D., Hammel, P. C. & Tsifrinovich, V. I. Solid-state nuclear-spin quantum computer based on magnetic resonance force microscopy. *Phys. Rev. B* **61,** 14694–14699 (2000).
15. Neumann, P. *et al.* Single-shot readout of a single nuclear spin. *Science* **329,** 542–544 (2010).
16. Bogani, L. & Wernsdorfer, W. Molecular spintronics using single-molecule magnets. *Nature Mater.* **7,** 179–186 (2008).
17. Friedman, J. R., Sarachik, M. P., Tejada, J. & Ziolo, R. Macroscopic measurement of resonant magnetization tunnelling in high-spin molecules. *Phys. Rev. Lett.* **76,** 3830–3833 (1996).
18. Thomas, L. *et al.* Macroscopic quantum tunnelling of magnetization in a single crystal of nanomagnets. *Nature* **383,** 145–147 (1996).
19. Wernsdorfer, W. & Sessoli, R. Quantum phase interference and parity effects in magnetic molecular clusters. *Science* **284,** 133–135 (1999).
20. Ardavan, A. *et al.* Will spin-relaxation times in molecular magnets permit quantum information processing? *Phys. Rev. Lett.* **98,** 1–4 (2007).
21. Bertaina, S. *et al.* Quantum oscillations in a molecular magnet. *Nature* **453,** 203–206 (2008).
22. Komeda, T. *et al.* Observation and electric current control of a local spin in a single-molecule magnet. *Nature Commun.* **2,** 217 (2011).
23. Otte, A. F. *et al.* The role of magnetic anisotropy in the Kondo effect. *Nature Phys.* **4,** 847–850 (2008).
24. Heersche, H. B. *et al.* Electron transport through single $Mn_{12}$ molecular magnets. *Phys. Rev. Lett.* **96,** 206801 (2006).
25. Zyazin, A. S. *et al.* Electric field controlled magnetic anisotropy in a single molecule. *Nano Lett.* **10,** 3307–3311 (2010).
26. Urdampilleta, M., Cleuziou, J.-P., Klyatskaya, S., Ruben, M. & Wernsdorfer, W. Supramolecular spin valves. *Nature Mater.* **10,** 502–506 (2011).
27. Park, H., Lim, A. K. L., Alivisatos, A. P., Park, J. & McEuen, P. L. Fabrication of metallic electrodes with nanometer separation by electromigration. *Appl. Phys. Lett.* **75,** 301–303 (1999).
28. Stepanow, S. *et al.* Spin and orbital magnetic moment anisotropies of monodispersed bis(phthalocyaninato)terbium on a copper surface. Supp. Inf. *J. Am. Chem. Soc.* **132,** 11900–11901 (2010).
29. Ishikawa, N., Sugita, M. & Wernsdorfer, W. Quantum tunneling of magnetization in lanthanide single-molecule magnets: bis(phthalocyaninato)terbium and bis(phthalocyaninato)dysprosium anions. *Angew. Chem. Int. Ed.* **44,** 2931–2935 (2005).
30. Abragam, A. *The Principles of Nuclear Magnetism* (Oxford Univ. Press, 1994).
31. Leuenberger, M. N. & Loss, D. The Grover algorithm with large nuclear spins in semiconductors. *Phys. Rev. B* **68,** 165317 (2003).


**Supplementary Information** is linked to the online version of the paper at www.nature.com/nature.

**Acknowledgements** We thank E. Eyraud, D. Lepoittevin, L. Cagnon, R. Haettel, C. Hoarau, V. Reita and P. Rodière for technical contributions and discussions. We thank T. Fournier, T. Crozes, B. Fernandez, S. Dufresnes and G. Julie for lithography development; E. Bonet, C. Thirion and R. Piquerel for help with software development and M. Urdampilleta, S. Thiele, N. Roch, A. Varlet and A. Ralko for discussions. Samples were fabricated in the Nanofab facility of the Néel Institute. This work is partially supported by the French National Research Agency National Programme in Nanosciences and Nanotechnologies (ANR-PNANO) project MolNanoSpin, number ANR-08-NANO-002; European Research Council Advanced Grant MolNanoSpin, number 226558; ICT-2007.8.0 Future Emerging Technologies Open, Quantum Information Processing Specific Targeted Research Project number 211284 MolSpinQIP; the German Research Foundation programme TRR 88 '3Met'; Cible 2009; and the Nanosciences Foundation of Grenoble.

**Author Contributions** R.V., W.W. and F.B. designed, conducted and analysed the experiments; S.K. and M.R. designed, synthesized and characterized the molecule; R.V., M.R., W.W., and F.B. co-wrote the paper.

**Author Information** Reprints and permissions information is available at www.nature.com/reprints. The authors declare no competing financial interests. Readers are welcome to comment on the online version of this article at www.nature.com/nature. Correspondence and requests for materials should be addressed to F.B. (franck.balestro@grenoble.cnrs.fr) or M.R. (mario.ruben@kit.edu).

doi:10.1038/nature11341

**Content**

## I. Molecular quantum devices: direct versus indirect coupling

It is very important to distinguish the type of devices fabricated in the field of molecular quantum spintronics. We distinguish here two classes with a read-out via a *direct* or *indirect coupling*. Since the latter method was used in the described measurements, the main arguments for this choice are given in the following.

### a) Direct coupling

In the beginning of the field of molecular spintronics, all the published devices were based on a direct coupling scheme, that is, the source-drain current was directly coupled to the spin system of the molecule [1,2]. A typical example concerns the electromigrated junction devices, which contain a gate electrode in addition to source and drain electrodes. Such a three-terminal transport device, called a *molecular spin-transistor*, is a single-electron transistor with non-magnetic electrodes and a single magnetic molecule as the island. The current flows from the source to the drain through the magnetic molecule, and the electronic transport properties are tuned using a gate voltage $V_g$. Two experimental regimes can be distinguished, depending on the coupling strength between molecule and electrodes. (i) In the weak-coupling limit, charging effects dominate the transport, revealing Coulomb-blockade, negative differential conductance, etc. (ii) For stronger electronic coupling between the molecule and the leads, higher-order tunnel processes become important, leading to elastic or inelastic cotunnelling processes and to Kondo effects. In both regimes, it was possible to find signatures of the magnetic spin states of the magnetic molecule [1, 2]. However, due to the direct coupling, the read-out is intertwined with a strong back-action, which will reduce relaxation and coherence times. In addition, in the strong coupling regime the magnetic properties of the molecule are strongly altered by hybridisation of the molecule orbitals with the metallic electrodes. To avoid such severe drawbacks, we decided to use an indirect coupling scheme in our work, which is discussed in the next paragraph.

### b) Indirect coupling

This situation describes double-dot devices with three terminals, where the current passes through one quantum dot (so-called read-out quantum dot, or shorter **read-out dot**, e.g. quantum wire, nanotube, organic ligand, etc.), while the magnetic information is stored on the second quantum dot (so-called **spin-dot**, e.g. magnetic molecule, metal ion, etc.) Although the two dots are only weakly coupled, the spin-dot can influence the transport properties of the read-out dot (see paragraph II). It allows the read-out of the spin-state of the spin-dot via the read-out dot with only minimal back-action.

Herein such a situation was realized by using the Pc ligands as read-out dot, which was directly

coupled to the leads (see the direct coupling). The spin-dot, formed by the magnetic Tb-ion, is only weakly coupled to the read-out dot. The read-out dot can be, with respect to the electrodes, in the intermediate or weak-coupling limit. Both regimes allow the **all-electronic** read-out of the Tb magnetic moment. The data presented in this work concern the intermediate coupling limit, that is, a weak spin $S = 1/2$ Kondo effect is observed (see below).

## II. Coupling between the read-out dot and the magnetic moment of the Tb ion

There are different possibilities to describe the coupling between the **read-out dot** (the Pc ligands in our work) and the **spin-dot** (the magnetic moment carried by the Tb-ion). We mention here 5 possibilities:

a) Dipole coupling
b) Exchange coupling [3]
c) Magneto-Coulomb coupling [4, 5]
d) Flux coupling [6]
e) Mechanical coupling [7]

### a) Dipole coupling

Here, we consider the dipolar field from the magnetic momentum of the $Tb^{3+}$ ion acting on the read-out dot. The exact evaluation of the dipole coupling is difficult because it has to take into account the 4f orbital geometry of the Tb electrons and the geometry of the read-out dot. Supposing that the magnetic momentum of $J \approx 6\ \mu_B$ is centred at the Tb ion, the magnetic field value acting at the Pc ligands, located 0.5 nm above and below the Tb ion, is about 60 mT. Moreover, the coupling between the magnetic momentum of the $Tb^{3+}$ ion and the read-out dot depends also on the spin-state of the latter. Because the read-out dot can be charged with an odd or even numbers of electrons (leading to different spin-states), the dipole coupling strength can be tuned by changing the back-gate voltage.

### b) Exchange coupling

The exchange coupling can be significantly strong as for instance in $N@C_{60}$, where the exchange coupling between a nitrogen atom and the electrons of the $C_{60}$ cage was found to be equal to 7 T [3,4]. Concerning $TbPc_2$, recent studies have shown a weak antiferromagnetic exchange coupling between the Tb magnetic moment and a ferromagnetic Ni-substrate [5]. Additionally, the organic radical ligand state of $S = 1/2$ is close in energy to the Tb-4f states [6] enabling an efficient coupling of the terbium magnetic moment $J = 6$ with the electrons responsible for the transport. In short, these

recent experiments and theoretical predictions suggest that there is probably a relatively larger exchange interaction between the magnetic momentum of the $Tb^{3+}$ ion and the 1/2 radical of the Pc ligands, with a coupling energy of about 0.3 T (see also Kondo effect analysis in paragraph III).

**c) Magneto-Coulomb coupling**

The magneto-Coulomb effect, reported in [7, 8], is based on the chemical potential variation of an 'isolated' magnetic system, due to the Zeeman energy, that is, a magnetic system gains (losses) energy when a magnetic field is applied along (opposite) to the magnetization. This change of energy can be probed by a single-electron transistor (SET) or a quantum dot (here called the read-out dot), which is weakly coupled to the magnetic system [7, 8].

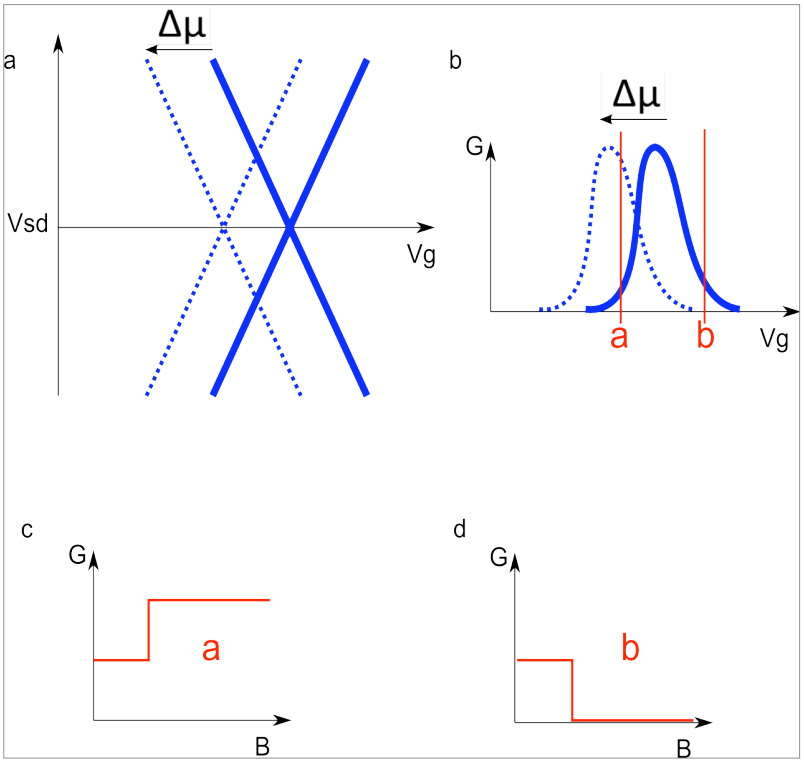


**Figure S1: Scheme of the magneto-Coulomb effect on the conductance.** The chemical potential variation Δμ, which is transferred from the spin-dot to the read-out dot, shifts the Coulomb diamonds **a**, leading to a shift of the Coulomb peaks depict in **b**. Therefore, the magnetization reversal of the spin-dot yields an increase (decrease) of the conductance $G$ versus the field $B$, when a gate voltage $V_g$ on the left (right) side of the Coulomb peak is applied, as shown in **c** and **d**, respectively.

In this case, a fraction of the chemical potential variation of the magnetic system is transferred to the read-out dot, leading to a shift of its Coulomb diamonds (see Fig. S1 and Fig. 4c of [8]). For an hysteretic magnetic system, this leads to a change of the sign of the conductance jump for measurements on the left or right side of the charge degeneracy point. For example, let us consider the

case where a Coulomb peak moves toward the lower gate value, Fig S1b. If one measures the conductance jump on the right side of the Coulomb peak, one should observe a negative conductance jump, whereas if one measures it on the left part, it should be positive as shown in the Fig S1c-d. Very importantly, the magneto-Coulomb effect predicts that the sign and the amplitude of the conductance jump depend also on the sign and amplitude of the magnetic field.

We performed measurements to monitor the sign of the conductance jump as a function of the gate voltage (Fig S2). Because we do not observe any sign change correlated to the position of the working point with respect to the charge degeneracy point, we conclude that the magneto-Coulomb effect is not a major contribution.

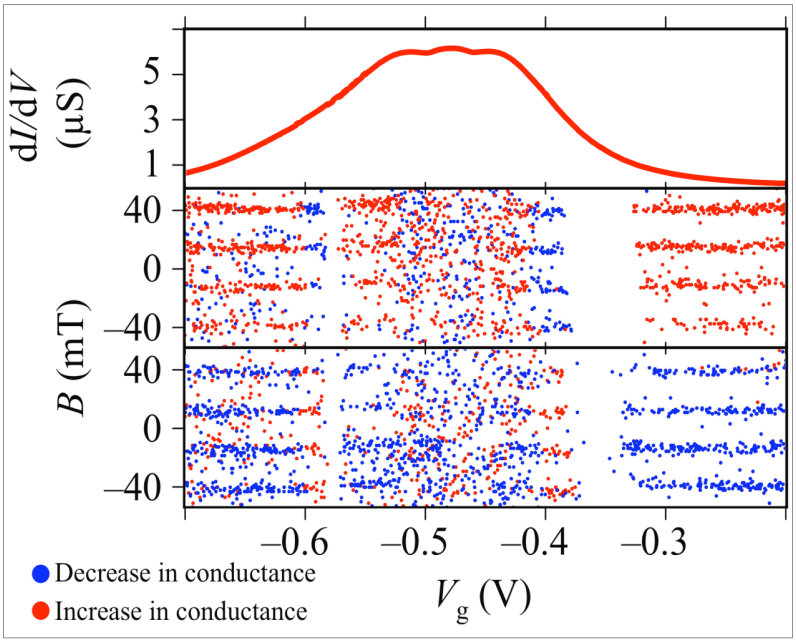


**Figure S2: Influence of the gate voltage on the sign of the conductance jumps.** In the upper part, the differential conductance at zero bias as a function of the gate voltage is shown. In the centre (bottom) part, the magnetic field values of the conductance jumps are plotted as a function of the gate voltage for the trace (retrace) field sweep. A blue point shows a decrease in conductance while a red one represents an increase. For both trace and retrace, the same sign of the conductance jumps is measured for the left and right side of the charge degeneracy point. Close to the degeneracy point, several sign changes are revealed. This complex behaviour needs further investigations. Note this measurements shows that sign of the jumps depends on the state of the magnetic moment of the $Tb^{3+}$ ion, i.e. the jump of the transition $J_z = 6$ to $J_z = -6$ has the opposite sign of $J_z = -6$ to $J_z = 6$.

**d) Flux coupling**

In order to detect the magnetic flux from the magnetic molecule, an appealing way is to use a carbon nanotube SQUID as a detector of the magnetic flux variation. For an in-depth discussion we would refer the reader to ref. [9].

**e) Mechanical coupling**

Rather recently, a new mechanical method has been proposed, which is based on the momentum conservation [10]. This conservation implies a rotation of the molecule to compensate for the reversal of its magnetic moment thus modifying the coupling to the electrodes. Even for small variations of the molecule orientation, the signal should be large enough to be measured; the tunnelling coupling (and therefore the current measured) depending exponentially on the distance between the molecule and the leads. In our case however, this explanation does not apply to the experimental situation, since it would be necessary to detect a rather sharp peak of conductance variation (instead of a step in our conductance curve), which should come from the fact that the molecule would tend to come back to its equilibrium position after the magnetization reversal. It would be therefore necessary to have fast amplifiers to detect such sharp conductance peaks. This mechanical method is certainly worth exploring in future set-ups.

## III. Experimental determination of the nature of the coupling using the Kondo effect

We studied the Kondo effect of the read-out dot as a function of both the magnetic field and the bias voltage (Fig. S3). Calculating the slope obtained from the Zeeman peaks, we have extracted a *g*-factor of 2 as expected for a $S = 1/2$ Kondo system. However, the extrapolation up to zero bias of the Zeeman peaks for positive values of the magnetic field gives a negative value for the critical field $B_c$ (Fig. S3). This is not expected for a $S = 1/2$ Kondo effect since the usual value is given by the relation:

$$2g\mu_B B_c = k_B T_K$$

where $g$ is the $g$-factor, $\mu_B$ is the Bohr magneton, $B_c$ is the critical field, $k_B$ is the Boltzmann constant and $T_K$ is the Kondo temperature. This discrepancy is attributed to an interaction between the spin $S = 1/2$ of the read-out dot with the magnetic moment of the $Tb^{3+}$ ion on the spin-dot. This configuration yields the new equation:

$$2g\mu_B B_c = k_B T_K + aJ_z$$

where $a$ is a positive constant accounting for the coupling between the magnetic moment of the $Tb^{3+}$ ion and the radical of the read-out dot, and $J_z$ is the $z$-component of magnetic moment of the $Tb^{3+}$ ion. Using the $B_c$ and $T_K$ values extracted from the measurements presented in Fig. S3, the interaction parameter $a$ is found to be equal to 350 mT.

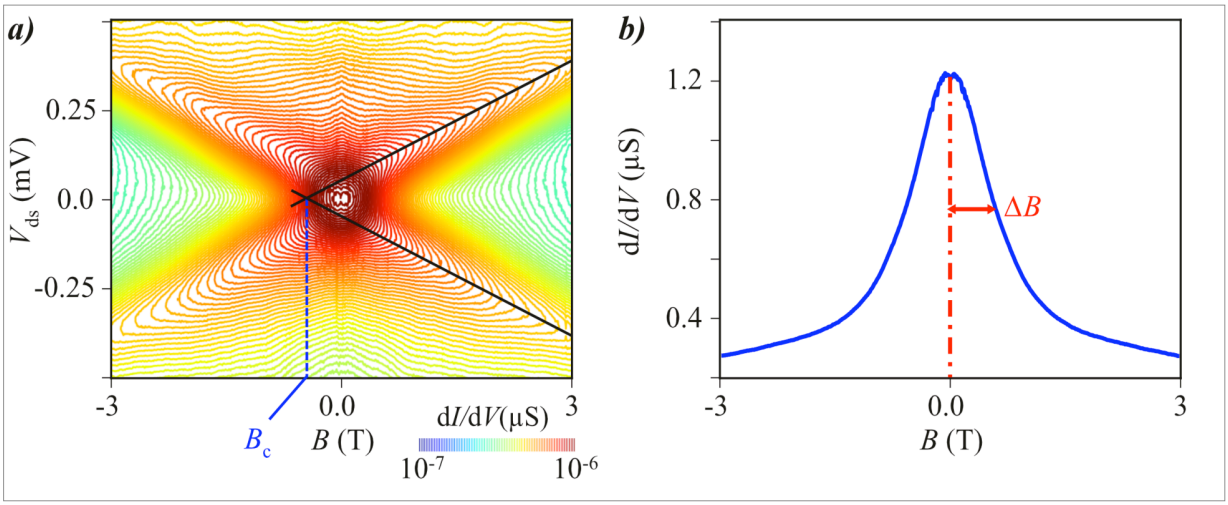


**Figure S3 : Kondo analysis of the read-out dot. a**, The contour plot of the differential conductance as a function of the magnetic field and the bias voltage performed on the Kondo ridge. The extrapolation of the Zeeman peaks at zero bias for positive values of the magnetic field gives the critical field $B_c$ = -0.4 T. **b**, The differential conductance as function of the magnetic field extracted from a at zero bias. The half-width can be used to estimate the Kondo temperature of $T_K$ = 0.6 T.

Such a high value is unlikely to be due to dipolar interaction alone (see paragraph II.a). We have to suppose that an exchange interaction (see paragraph II.b) is also involved in the coupling and even dominates it. According to the shift direction of the critical field $B_c$, we can deduce that this exchange interaction is ferromagnetic. Furthermore, such a high coupling strength is only possible if the read-out dot is very close to the spin-dot. Thus, we conclude that the Pc-ligand acts as a read-out dot and electron transport takes place through the Pc-ligand of the $TbPc_2$ molecule, as depicted in Fig. 1a of the main text.

The local magnetic field felt by the read-out dot has two contributions: (i) the magnetic field applied to the sample using the 3-D vector magnets and (ii) the magnetic coupling with the magnetic moment of the $Tb^{3+}$ ion. For a given $J_z$ state ($J_z = \pm 6$), the local magnetic field will vary according to the applied magnetic field, while the coupling with the $Tb^{3+}$ ion will only induce an offset. The conductance does not present an abrupt jump while sweeping the applied magnetic field unless the magnetic moment of the $Tb^{3+}$ ion reverses. The local magnetic field of the read-out dot varies then abruptly, inducing an abrupt shift of its chemical potential energy, which leads to a jump of the

conductance through the read-out dot.

In summary, the magnetization reversal of the spin-dot induces an abrupt variation of the local effective magnetic field felt by the read-out dot. Its chemical potential will then shift, revealed by an abrupt jump of the conductance through the read-out dot.

## IV. Magnetic field alignment

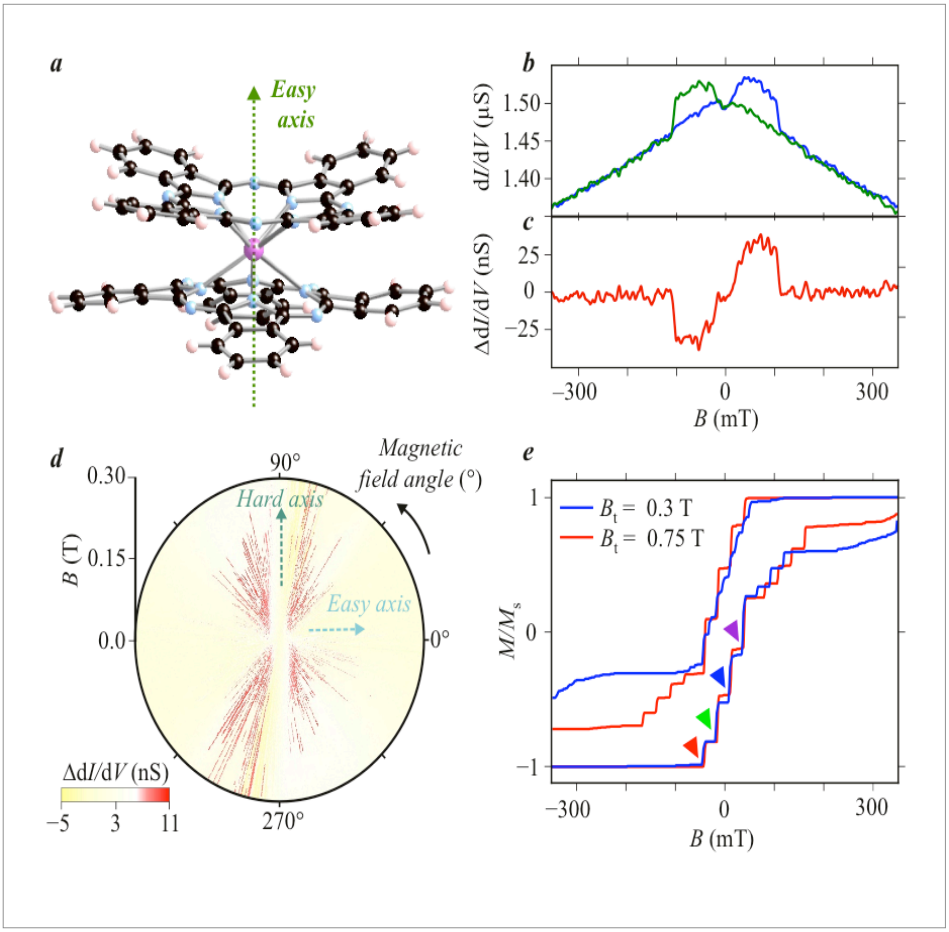


**Figure S4 Determination of the $TbPc_2$ easy axis orientation with respect to the experimental setup. a,** Molecule structure of the $TbPc_2$-SMM showing its easy axis of magnetization perpendicular to the Pc plane. **b,** The differential conductance d*I*/d*V* is measured while sweeping the magnetic field back and forth. Conductance jumps are observed, which are attributed to the reversal of the magnetic moment of the $TbPc_2$-SMM. **c,** Difference of d*I*/d*V* between the trace and retrace yielding the hysteresis of conductance Δ(d*I*/d*V*). **d,** Angular dependence of the hysteresis of conductance. **e** Normalized hysteresis loop of a single $TbPc_2$-SMM obtained by integration of about 1000 field sweeps, measured in the presence of two different fixed transverse magnetic fields $B_t$. The four QTM transitions of the $TbPc_2$-SMM are indicated. The other steps are due to direct transitions stimulated by a spin 1/2 system coupled to the Tb ion.

The magnetic moment of the $TbPc_2$-SMM has a preferential orientation (known as easy axis of

magnetization) due to its uniaxial magnetic anisotropy, which is oriented perpendicular to the Pc plane (see main text and Fig. S5a). The field sweep direction has to be aligned with the easy axis, *i.e.* it is important to determine the relative orientation of the molecule with respect to the magnetic field coils. Our dilution refrigerator is equipped with a home-made two-dimensional vector magnet and it is possible to rotate the refrigerator along one of the magnetic field coil axes. Thus, this particular set-up allows us to study the magnetic response in three dimensions.

In order to determine the orientation of the molecule, we first performed differential conductance hysteresis loops (Fig. S5b) at different applied field angles. The conductance hysteresis $\Delta(\mathrm{d}I/\mathrm{d}V)$ was then plotted by taking the difference between the trace and retrace (Fig. S5c). Fig. S5d presents the polar representation of $\Delta(\mathrm{d}I/\mathrm{d}V)$ as a function of the angle. It yields one direction in the hard plane and the projection of the easy axis in the measured magnetic field plane. Then after a rotation of the dilution refrigerator, the angle dependence of $\Delta(\mathrm{d}I/\mathrm{d}V)$ is measured again in the new plane in order to find a second direction in the hard plane. Finally, the vector product of the two hard axes direction yields the easy axis direction.

The alignment can be confirmed by measuring the hysteresis loop of the molecule as a function of a constant magnetic field applied transverse to the easy axis direction (Fig. S5e). If the alignment is correct, the position of the steps at small magnetic fields, associated to QTM of the $TbPc_2$-SMM, should not depend on the transverse field, which is the case for our sample confirming the quality of our alignment. The steps measured at higher magnetic fields correspond to the influence of a spin 1/2 system, which stimulates a direct transition of the $TbPc_2$-SMM. Such stimulated direct transitions are beyond the scope of this work.

## V. Comparaison between single-molecule and molecule ensemble measurements

Fig. S5 compares the hysteresis loops of the single-molecule measurements (main text) with molecule ensemble measurements performed on a crystal of $YPc_2$ (diamagnetic) doped with 2% of $TbPc_2$, using the micro-SQUID technique [11]. Both hysteresis loops present a clear staircase-like structure at small magnetic fields, which indicates the occurrence of QTM. At higher magnetic fields, the reversal of the magnetization occurs via a direct relaxation process involving tunnelling and phonon emission. The four QTM transitions of the $TbPc_2$-SMM are indicated in both figures. Note, however, that the ensemble measurement shows other steps in between the four QTM transitions, which are probably induced by spin-spin interactions [12].

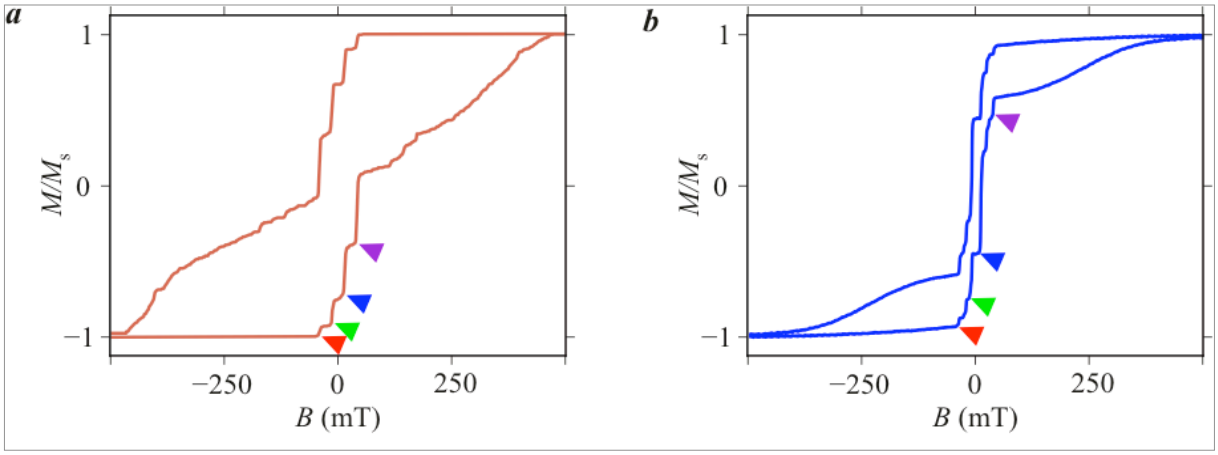


**Figure S5 Comparison of the hysteresis loops of a single-molecule and an ensemble of $TbPc_2$ molecules. a,** Normalized hysteresis loop of a single $TbPc_2$-SMM obtained by integration of about 1000 field sweeps. **b,** Hysteresis loop for a single crystal of $YPc_2$ doped with 2% of $TbPc_2$ at 0.04 K. In both cases the applied magnetic field was aligned along the easy axis of magnetization.

## VI. Robustness of the nuclear spin-state with regards to our measurement procedure

In the main text, we present an estimation of the lifetime of one single nuclear spin by measuring the evolution of the nuclear spin-state population for different waiting times between two measurements. In order to assess the robustness of the nuclear spin-states with regards to our measurement procedure, we have also monitored the evolution of the transition matrices after different numbers of measurements. This evolution was obtained by measuring the nuclear spin-state correlation between an initial nuclear spin-state, measured by sweeping the magnetic field, and the nuclear spin-state obtained after the $n^{th}$ measurement, without waiting time. If the measurement procedure were to perturb the nuclear spin-state, a predominance of the off-diagonal terms would be expected for $n \geq 2$, as the off-diagonal correlation terms account for the nuclear spin-states, which relaxed or were excited between the two measurements ($\Delta m = \pm 1, \pm 2, \pm 3$). On the other hand, if the nuclear spin-states were only slightly perturbed, one would expect that the diagonal terms remain predominant.

Fig. S6 presents the evolution of the transition matrix as a function of the number of measurements $n$. It is observed that the diagonal elements persist even after several measurements clearly enlightening the low invasive measurement procedure that uses the detection of QTM as a probe of the nuclear spin-state. Note that the appearance of the off-diagonal elements is comparable to the waiting time measurement (Fig. 3), knowing that each field sweep takes about 5 s, that is $n = 1$, $n = 10$ corresponds to a waiting time $t_w = 50$ s.

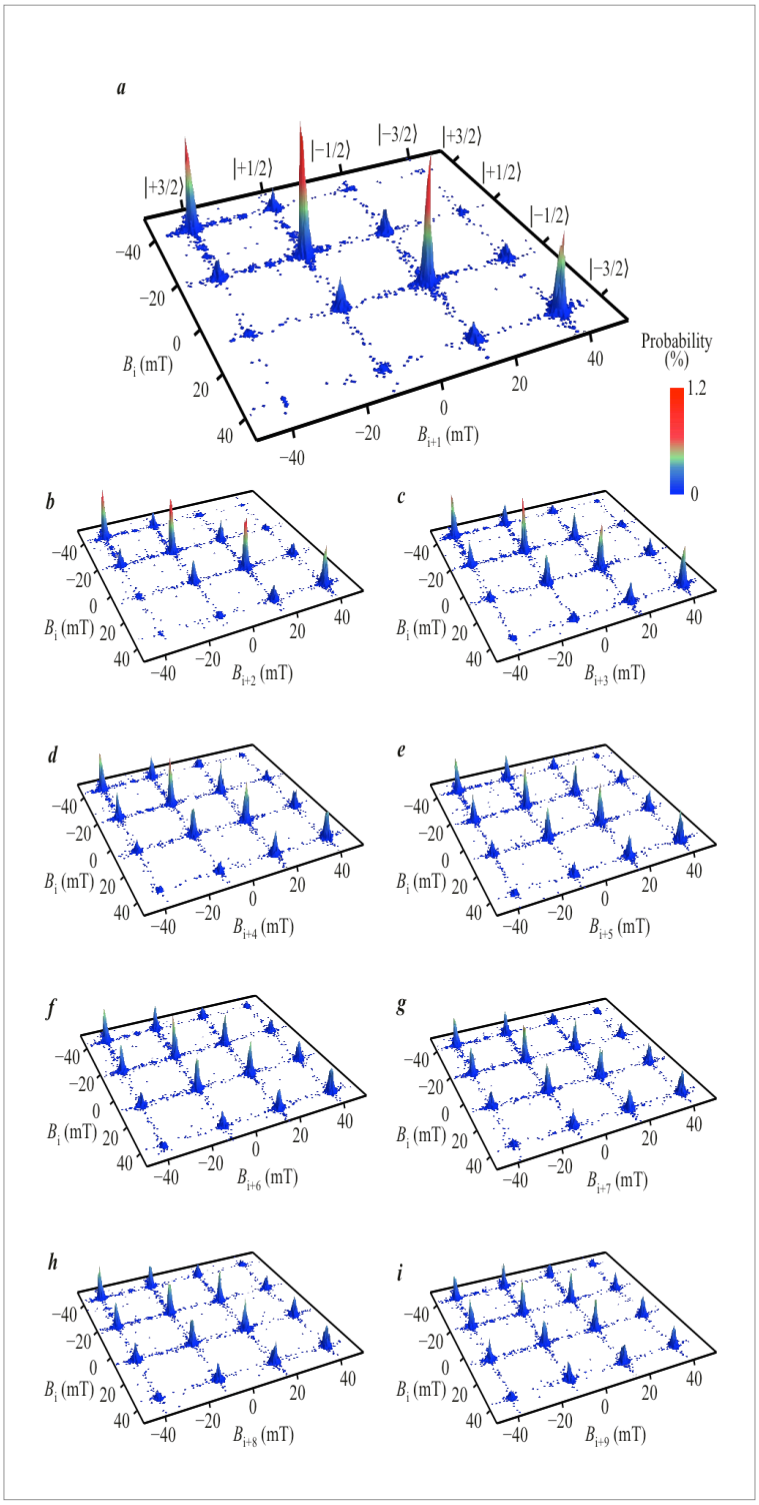


**Figure S6: Evolution of the transition matrix. a,** Spin state correlation between two consecutive measurements. The predominance of the diagonal terms demonstrates that the nuclear spin did not change its quantum state between the two measurements. **b – i,** Spin state correlation between the measurements $i$ and $i+n$ with $n$ = 2, 3, …, 10. The off-diagonal terms are only slowly appearing, showing the robustness of the nuclear spin state with respect to the measurement procedure.

## VII. The Hyperfine structure of the $Tb^{3+}$ ion

In order to describe the hyperfine structure of the $Tb^{3+}$ ion, three contributions have to be included in the effective spin Hamiltonian for the calculation of the Zeeman diagram (Fig. S7a). The first one accounts for the hyperfine coupling between the nuclear spin $I = 3/2$ and the magnetic moment $J_z$ = +- 6 of the electrons. This first contribution can be written as:

$$H_{hyp} = aJ_z I_z$$

where $a$ is the hyperfine coupling strength, $J_z$ is the z component of the electronic magnetic moment and $I_z$ the one of the nuclear magnetic moment.

The second contribution accounts for the quadrupole moment of the nuclear spin. It originates from the non-perfectly spherical shape of the nucleus and can be expressed as:

$$H_{quad} = P\left(I_z^2 - \frac{1}{3} I(I+1)\right)$$

where $P$ is the quadrupole moment of the nucleus and where a constant has been added to fulfill $\mathrm{tr}(H_{quad}) = 0$.

The last contribution is the Zeeman term that can be neglected due to the small gyromagnetic moment of the nucleus.

MicroSquid measurements were previously performed on molecular crystals by Ishikawa *et al.* [10] to determine the two coefficients $a$ and $P$. They were found to be equal to $0.01 cm^{-1}$ and $0.013 cm^{-1}$ respectively. Using these values, the energy differences between the nuclear spin-states have been calculated as presented in Fig. S7b.

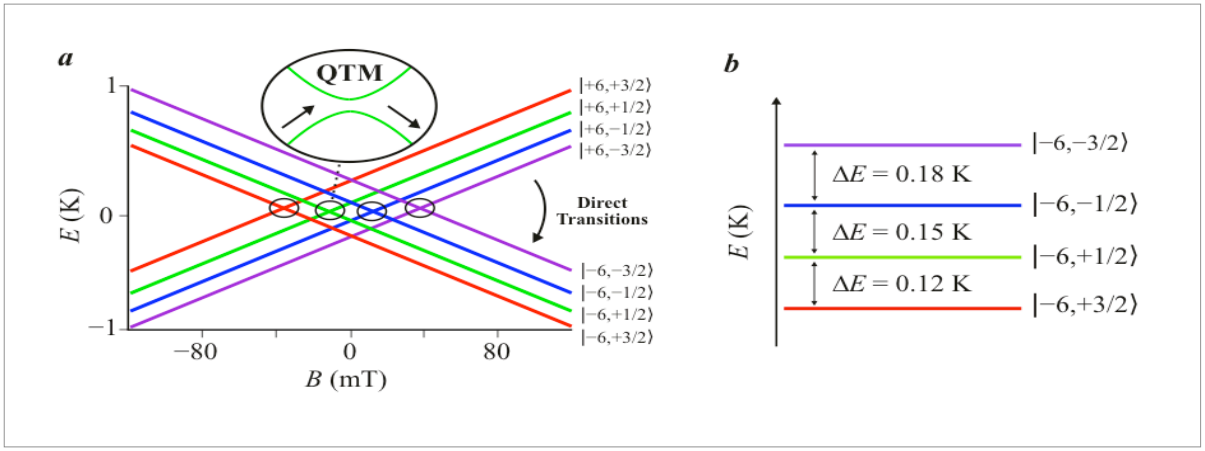


**Figure S7 : Nuclear spin-state energies. a,** Zeeman diagram presenting the energy of the two ground states $J_z = \pm 6$ as a function of the magnetic field. The two ground states are both split into four different sub-states due to the hyperfine coupling with the nuclear spin of $I = 3/2$. The violet, blue, green and red colours account for the $I_z$ component -3/2, -1/2, 1/2 and 3/2 of the nuclear spin states, respectively. **b,** Energy differences between nuclear the spin-states for the electronic magnetic moment $J_z = -6$ and at small magnetic fields.

## VIII. Bibliography


[1] Heersche, H. *et al.* Electron Transport through Single Mn12 Molecular Magnets. *Phys. Rev. Lett.* **96**, 206801 1-4 (2006).

[2] Jo., M. H. *et al.* Signatures of molecular magnetism in single-molecule transport spectroscopy. *Nano Letters* **6**, no. 9, 2014-2020 (2006).

[3] Grose, J. E. *et al.* Tunnelling spectra of individual magnetic endofullerene molecules. *Nature Materials* **7**, 884-889 (2008).

[4] Roch, N. *et al.* Cotunneling through a magnetic single-molecule transistor based on N@$C_{60}$. *Phys. Rev. B* **83**, 081407(R) 1-4 (2011).

[5] Lodi Rizzini, A. *et al.* Coupling Single Molecule Magnets to Ferromagnetic Substrates. *Phys. Rev. Lett.***107**, 177205 1-5 (2011).

[6] Vitali, L. *et al.* Electronic structure of surface-supported bis(phthalocyaninato) terbium(III) single molecular magnets. *Nano Letters* **8**, 3364-3368 (2008).

[7] Cleuziou, J.-P., Wernsdorfer, W., Ondarçuhu, T. & Monthioux, M. Electrical detection of individual magnetic nanoparticles encapsulated in carbon nanotubes. *ACS Nano* **5**, 2348-2355 (2011).

[8] Datta, S. *et al.* Magneto-Coulomb Effect in Carbon Nanotube Quantum Dots Filled with Magnetic Nanoparticles. *Phys. Rev. Lett.* **107**, 186 804 1-4 (2011).

[9] Cleuziou, J. P., Wernsdorfer, W., Bouchiat, V., Ondarçuhu, T. and Monthioux, M. (2007), Carbon nanotube based magnetic flux detector for molecular spintronics. *Phys. Status Solidi B*, **244**, 4351–4355.

[10] Jaafar, R., Chudnovsky, E.M. & Garanin, D. a. Single magnetic molecule between conducting leads: Effect of mechanical rotations. *EPL (Europhysics Letters)* **89**, 27001 (2010).

[11] Ishikawa, N., Sugita, M. & Wernsdorfer, W. Quantum tunneling of magnetization in lanthanide single-molecule magnets: bis(phthalocyaninato)terbium and bis(phthalocyaninato)dysprosium anions. *Angew. Chem. (Int. Ed.)* **44**, 2931-2935 (2005).

[12] Wernsdorfer, W., Bhaduri, S., Tiron, R., Hendrickson, D. H., & Christou G. Spin-Spin Cross Relaxation in Single-Molecule Magnets. *Phys. Rev. Lett.* **89**, 197201 (2002).